Politecnico di Torino

Analysis of a Bulk-Mediated Surface Diffusion Model to Interprete Experimental Observations

an M2 internship authored by
Joan Descoubes

supervised by
Thomas Guerin and Luca Dall'Asta

done at
Laboratoires Ondes et Matière d'Aquitaine
CNRS/Université de Bordeaux
351 cours de la Libération, Talence, France

19 June, 2025

Contents

Chapter 1

Introduction

1.1 Context and motivations

The stochastic motion of tracer particles in complex media has been the focus of many recent studies [6, 7, 13]. One important example of complex stochastic motion is in the presence of obstacles, as in porous media or micro-channels, where diffusion is slowed-down by entropic traps [10]. While the majority of studies consider reflecting walls, the tracer particle can also interact with the walls, and, in the case of small range attraction, switch between attached and detached states. This type of motion also plays a key role in first passage problems, where it has been shown to enhance particle dispersion in undulating microchannels [2]. Additionally, it was found that boundary excursions can accelerate search processes in circular domains [5]. A minimal theoretical framework capturing this behavior is Bulk-Mediated Surface Diffusion (BMSD): particles temporarily attach to the surface (adsorption), then detach (desorption), diffuse in the bulk medium (e.g., a liquid), and re-adsorb. The trajectory between the desorption and the subsequent adsorption is called a flight [14].

This type of motion has recently been observed experimentally using Total Internal Reflection Fluorescence Microscopy (TIRFM) techniques, in which the motion can be observed only near the walls [11, 12, 16], and more recently, through 3D single-molecule imaging methods [15].

However, no existing theory fully explains the experimental observations, and there is currently no reliable method for extracting the adsorption and desorption rates. In particular, experimental results show that the waiting times (between adsorption and desorption) are not exponentially distributed, and the measured Mean Square Displacement (MSD) is either diffusive or subdiffusive — while theoretical arguments predict a scaling of MSD $\sim t^{3/2}$ with time t in some regime [4]. In another theoretical study, the MSD $\sim t^{5/2}$ is found at short times and linear at long times with a diffusion coefficient different from the bulk one [3].

The goal of this internship is to re-examine the properties of diffusion near a sticky (and flat) surface, and to predict the quantities that are effectively measured in TIRF experiments, to enable the determination of the attachment/detachment rates. In particular, the following questions are asked :

1. Can experimental waiting times be used to estimate the model parameters?
2. In which regime superdiffusion appears and with what exponent ? Can we provide an explanation for the Mean-Square Displacement obtained experimentally ?
3. Can the surface distribution of particles be characterised ? And in which regime is it non-Gaussian ?

The outline of this report is as follows. First, in the rest of this chapter, the experimental results that one aims to explain are presented, and I introduce the model (with the results that had already been obtained before the internship). Then, in chapter 2 the analytical expressions for the apparent waiting times (average and tail of the distribution) are checked. Finally, in chapter 3 the mean square displacement and the surface distribution are characterised in different limits.

1.2 Single-Molecule Tracking of Polymer Surface Diffusion

The article *"Single-Molecule Tracking of Polymer Surface Diffusion"* [12] reports an experiment in which only intermittent immobilisation and desorption-mediated displacements were observed; the surface diffusion coefficient was below the detection limit, ($D_s < 0.002\,\mu\mathrm{m}^2/\mathrm{s}$). Polymers of various Molecular Weights (MW) were tracked at the aqueous-solution/solid interface. Because diffusion in the bulk phase is rapid, ($D > 10\,\mu\mathrm{m}^2/\mathrm{s}$, as reported in the Supplementary Information of the article), single-molecule tracking was restricted to periods when the polymers were adsorbed. Trajectories were reconstructed by linking nearest-neighbour positions in consecutive images. A maximum displacement of $R_{\max} = 2.2\,\mu\mathrm{m}$ was allowed between successive adsorption events (to be reasonably sure that the same particle attached).

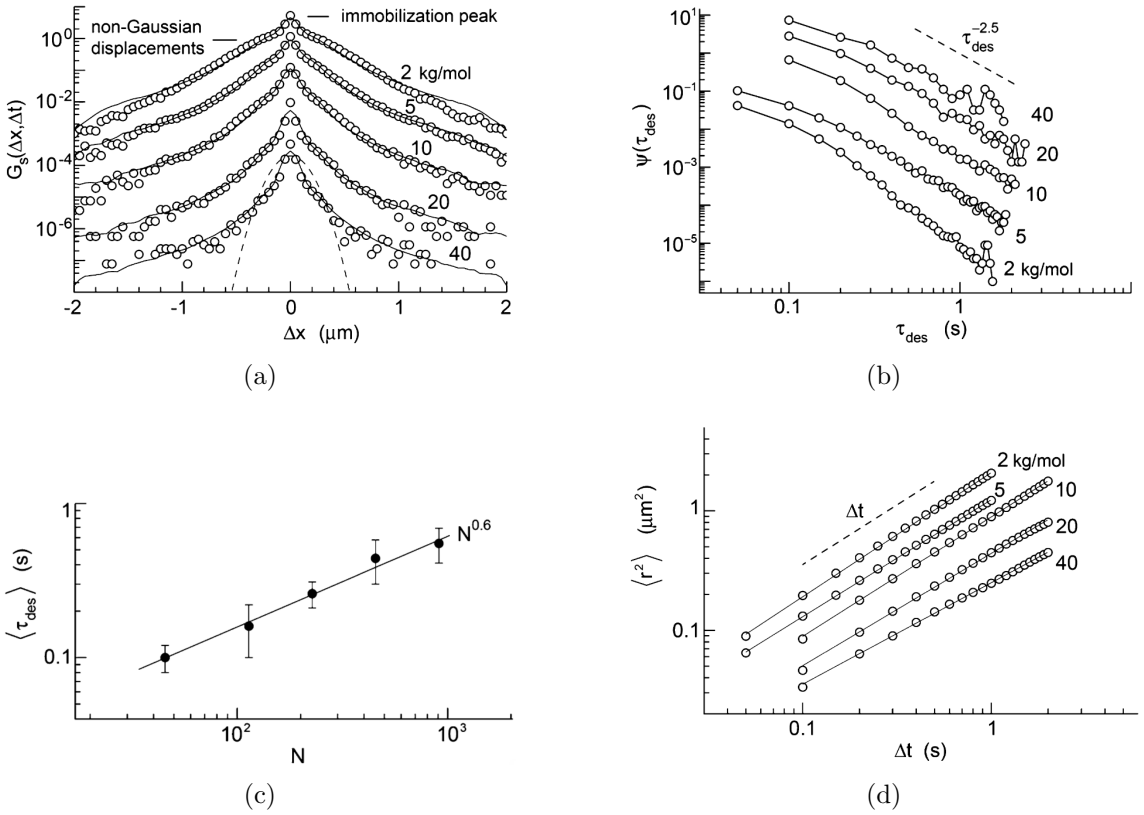

Figure 1.1: Experimental results from the article [12] (a) Experimental distribution of surface displacements (represented by circles) for a time interval $\Delta t = 0.1\,\mathrm{s}$; (b) Distribution of desorption times; (c) Average waiting time as a function of chain length N; (d) Mean square displacement as a function of time Δt. The curves in (a) and (b) were vertically shifted for clarity. In (a), (b) and (d) the different curves correspond to different molecular weights of the tracer.

Figure 1.1(a) shows the distribution of surface displacements. The distributions are clearly non-Gaussian and become increasingly peaked with growing MW.

The waiting-time distribution between desorption-mediated flights is shown in Figure 1.1(b). Tracers were considered as having desorbed once displaced of a length $r > R$ with $R = 0.2\,\mu m$. The distribution exhibits a power-law tail: $\psi(\tau) \propto \tau^{-5/2}$.

The average waiting time as a function of MW is shown in Figure 1.1(c).

Finally, the mean-square displacement (MSD) curves (see, Figure 1.1(d) are approximately linear, with effective diffusion coefficients ranging from 0.05-1 μm^2/s, much bellow the bulk diffusion coefficient.

1.3 Theoretical model

In this section, we present the theoretical model to describe bulk-mediated surface diffusion (BMSD). The model has three parameters κ, k_d and D (but to estimate this last parameter from experiments, standard methods already exist).

Note that, although κ is called attachment rate, it has dimensions of a velocity. Moreover, it is the same parameter as the "reactivity parameter" in studies of transport influenced reactions [9].

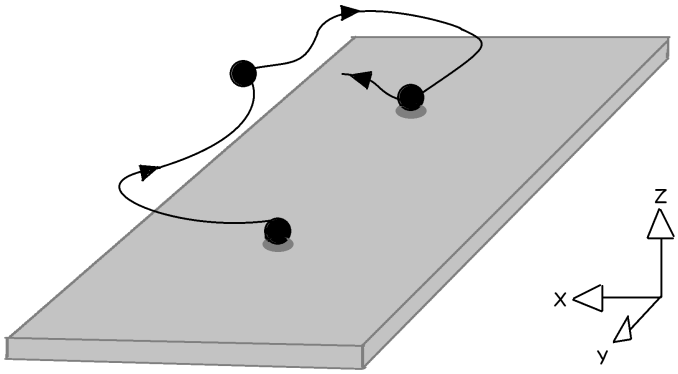

Figure 1.2: Schematic representation of the bulk-mediated surface diffusion mechanism. A particle desorbs from the surface, diffuses in the bulk, and subsequently re-adsorbs at a different surface location.

1.3.1 First formulation

The first formulation consists in considering trajectories as a succession of phases in the bulk or in the adsorbed state.

In the following, z is the distance to the wall and x, y are the in plane cartesian coordinates. A planar wall is located at $z = 0$, to which a particle is initially adsorbed at the origin ($x = y = 0$). Surface diffusion is neglected ($D_s = 0$). After a random residence time t, drawn from an exponential distribution,

$$\psi_d(t) = k_d e^{-k_d t}, \tag{1.1}$$

the particle desorbs from the surface and diffuses freely in the bulk for a time t', after which it re-adsorbs to the surface. This process can be iterated and is illustrated in Fig. 1.2.

The displacement PDF in the x-direction between the desorption and readsorption events, knowing that a time t' is spent in the bulk, is given by a Gaussian distribution:

$$Q(x|t', x_d) = \frac{1}{\sqrt{4\pi D t'}} \exp\left(-\frac{(x - x_d)^2}{4Dt'}\right), \tag{1.2}$$

where x_d is the coordinate along the x-axis before desorption, and D is the bulk diffusion coefficient. The same applies independently in the y-direction.

To determine the distribution $g(t')$ of bulk diffusion times, consider a 1D diffusion process along the z-axis. The particle starts at $z = 0$ and diffuses with diffusion constant D. The boundary at $z = 0$ is partially absorbing and is described by Equation (1.5).

The system is governed by the following equations:

$$\partial_t p(z, t) = D\partial_z^2 p(z, t), \tag{1.3}$$

$$p(z, t = 0) = \delta(z), \tag{1.4}$$

$$D \left.\frac{\partial p}{\partial z}\right|_{z=0} = \kappa\, p(0, t) \tag{1.5}$$

where $p(z, t)$ is the probability density to be in the bulk at time t and position z, without having been adsorbed before t.

By taking the Laplace transform of this set of equations, then using the equality $g(t) = -\frac{\partial}{\partial t}\int_0^\infty dz\, p(z, t)$ and finally taking the inverse Laplace transformation, the following expression can be obtained for $g(t)$ (see section A.1, for the detailed calculation):

$$g(t) = \frac{\kappa^2}{D}\left[\frac{\sqrt{D}}{\sqrt{\pi\kappa^2 t}} - \mathrm{erfcx}\left(\sqrt{\frac{\kappa^2 t}{D}}\right)\right], \tag{1.6}$$

where $\mathrm{erfcx}(x) = e^{x^2}\,\mathrm{erfc}(x)$ is the scaled complementary error function.

Since in the experiments one does not have access to the true desorption time, but to an apparent one, we want to compute the distribution $\psi(T)$ for the apparent waiting time T. It is defined as the time it takes for a particle to be re-adsorbed at a distance $r > R$ from its initial location. More precisely, we define T as the time at which the particle was last observed on the surface before such a flight. Because an exact analytical expression is difficult to obtain, $\psi(T)$ is approximated by the effective distribution $\psi_e(t)$ defined as the time PDF before the particle does a flight of size $r > R$ for the first time. This approximation will be tested in chapter 2.

After some calculations, see section A.2, the following expression is obtained for the Laplace transform of $\psi_e(t)$:

$$\tilde{\psi_e}(s) = \frac{P\,\tilde{\psi_d}(s)}{1 - (1 - P)\tilde{\psi_d}(s)\tilde{p}(s)}, \tag{1.7}$$

where $\tilde{f}(s) = \int_0^\infty dt\, f(t)e^{-st}$ is the Laplace transform of $f(t)$,

$$p(t) = \frac{g(t)}{1 - P}\int_{x^2+y^2<R^2} dxdy\; Q(x|t)Q(y|t) = \frac{g(t)}{1 - P}\left(1 - \exp\left(-\frac{R^2}{4Dt}\right)\right) \tag{1.8}$$

is the probability density of attachment time given that the flight size is $r < R$, and

$$P = \int_{x^2+y^2>R^2} dxdy \int_0^\infty dt\; g(t)Q(x|t)Q(y|t) = \int_0^\infty dt\; g(t)e^{-R^2/(4Dt)} \tag{1.9}$$

is the probability of a flight of length larger than R.

This formulation will allow us to derive expressions for the behavior of the tail of the waiting-time distribution and for the effective average waiting time.

1.3.2 Second formulation

An equivalent formulation of the model is now presented, which will allow us to derive the surface distribution and the Mean-square displacement (MSD), see chapter 3.

Let $p_b(\underline{r}, z, t)$ be the probability density in the bulk, at position $\underline{r} = (x, y)$ and distance z, and $p_s(\underline{r}, t)$ on the surface. The particle starts at $\underline{r} = (0, 0)$ on the surface. The system evolves according to:

$$\partial_t p_b = D\left(\nabla_{\underline{r}} + \partial_z^2\right) p_b \qquad \text{for } z > 0, \tag{1.10}$$

$$\partial_t p_s = -k_d\, p_s + \kappa\, p_b \qquad \text{at } z = 0, \tag{1.11}$$

$$D\left.\frac{\partial p_b}{\partial z}\right|_{z=0} = \kappa\, p_b(\underline{r}, 0, t) - k_d\, p_s(\underline{r}, t), \tag{1.12}$$

$$p_s(\underline{r}, 0) = \delta(\underline{r}), \tag{1.13}$$

$$p_b(\underline{r}, z, 0) = 0. \tag{1.14}$$

Taking the Laplace transform in time and the Fourier transform in space yields:

$$\tilde{\tilde{p}}_s(\underline{k}, s) = \frac{1}{s + \dfrac{k_d D\sqrt{\underline{k}^2 + s/D}}{\kappa + D\sqrt{\underline{k}^2 + s/D}}}, \tag{1.15}$$

where $\hat{f}(\underline{k}) = \int d\underline{r}\, f(\underline{r}) e^{-i\underline{k}\cdot\underline{r}}$ is the Fourier transform of $f(\underline{r})$. The detailed calculation is given in section A.4.

In the next chapters, we will analyse these formulas to derive some properties of the apparent waiting times and of the surface distribution.

Chapter 2

Properties of apparent waiting times

In this chapter the properties of apparent waiting times are investigated. More specifically, we will focus on the average waiting time and the tail of the waiting time distribution.

2.1 Average waiting time

Since an apparent average waiting time can be measured experimentally, it is useful to derive an analytical expression to extract the model parameters corresponding to experimental conditions.

The effective average waiting time τ_e, associated to the distribution $\psi_e(t)$, can be obtained using $\tau_e = -\left.\frac{\partial \tilde{\psi}_e(s)}{\partial s}\right|_{s=0}$ and is given by:

$$\tau_e = n_e\,\tau_d + \tau_e^0, \tag{2.1}$$

where

$$n_e = \frac{1}{P} \tag{2.2}$$

is the average number of desorption events before a flight of size r larger than R, $\tau_d = \frac{1}{k_d}$ is the average waiting time to desorb from the surface and

$$\tau_e^0 = n_e \int_0^\infty dt\, t\, g(t) \left(1 - e^{-\frac{R^2}{4Dt}}\right) \tag{2.3}$$

is the effective average waiting time for $\tau_d = 0$.

2.1.1 Analytical analysis

The Π theorem is used to adimensionalize τ_e using D and R, leading to

$$\tau_e(\kappa, D, R, k_d) = \frac{R^2}{D}\,\tilde{\tau}_e(\tilde{\kappa}, \tilde{k}_d), \tag{2.4}$$

where $\tilde{\kappa} = \frac{\kappa R}{D}$ and $\tilde{k}_d = \frac{k_d R^2}{D}$. Moreover,

$$\tilde{\tau}_e(\tilde{\kappa}, \tilde{k}_d) = n_e(\frac{1}{\tilde{k}_d} + I), \tag{2.5}$$

where $I = \int_0^\infty dt\, \tilde{g}(t)(1-e^{-\frac{1}{4t}})t$, $n_e = 1/\int_0^\infty dt\, \tilde{g}(t)e^{-\frac{1}{4t}}$ and $\tilde{g}(t) = \tilde{\kappa}^2 \left(\frac{1}{\sqrt{\pi t\tilde{\kappa}^2}} - \mathrm{erfcx}(\sqrt{\tilde{\kappa}^2 t})\right)$.

Let us evaluate I and n_e in the limits $\kappa \to 0$ and $\kappa \to \infty$. In the limit $\tilde{\kappa} \to 0$ we have :

$$\begin{aligned} I &\overset{t''=\tilde{\kappa}^2 t}{=} \int_0^\infty \frac{dt''}{\tilde{\kappa}^2}\tilde{\kappa}^2 \left(\frac{1}{\sqrt{\pi t''}} - \mathrm{erfcx}(\sqrt{t''})\right)\left(1 - e^{-\frac{\tilde{\kappa}^2}{4t''}}\right)\frac{t''}{\tilde{\kappa}^2} \\ &\overset{\tilde{\kappa}\to 0}{=} \int_0^\infty dt'' \left(\frac{1}{\sqrt{\pi t''}} - \mathrm{erfcx}(\sqrt{t''})\right)\frac{1}{4} = \frac{1}{4}, \\ n_e &\overset{t''=\tilde{\kappa}^2 t}{=} 1/\int_0^\infty \frac{dt''}{\tilde{\kappa}^2}\tilde{\kappa}^2 \left(\frac{1}{\sqrt{\pi t''}} - \mathrm{erfcx}(\sqrt{t''})\right) e^{-\frac{\tilde{\kappa}^2}{4t''}} \overset{\tilde{\kappa}\to 0}{=} 1. \end{aligned}$$

In the opposite limit $\tilde{\kappa} \to \infty$,

$$\begin{aligned} I &\overset{\tilde{\kappa}\to\infty}{=} \int_0^\infty dt\, \frac{1}{2\sqrt{\pi}\tilde{\kappa}t^{3/2}}\left(1 - e^{-\frac{1}{4t}}\right)t = \frac{1}{2\tilde{\kappa}}, \\ n_e &\overset{\tilde{\kappa}\to\infty}{=} 1/\int_0^\infty dt\, \frac{1}{2\sqrt{\pi}\tilde{\kappa}t^{3/2}} e^{-\frac{1}{4t}} = \tilde{\kappa}. \end{aligned}$$

The resulting expression is:

$$\tilde{\tau}_e^0 = n_e\, I = \begin{cases} \frac{1}{4}, & \text{for } \tilde{\kappa} \to 0, \\ \frac{1}{2}, & \text{for } \tilde{\kappa} \to \infty. \end{cases} \tag{2.6}$$

and

$$n_e = \begin{cases} 1, & \text{for } \tilde{\kappa} \to 0, \\ \tilde{\kappa}, & \text{for } \tilde{\kappa} \to \infty. \end{cases} \tag{2.7}$$

As a consequence, in the limit $\tilde{\kappa} \to 0$ and when $\frac{R^2}{D} \ll \tau_e$, the average waiting time becomes independent of κ and $\tau_e \simeq \frac{1}{k_d}$.

2.1.2 Numerical Simulations

To verify whether the analytical expression of the average τ_e given in Equation (2.1) is a good approximation or not, numerical simulations are performed. These consist in generating waiting times in the bulk drawn from $g(t')$, but also flight sizes from $Q(x|t', x_d)$ and $Q(y|t', x_d)$. The trajectories were generated until the distance from the initial position is larger than R (thus giving τ, the apparent average waiting time, associated to distribution $\psi(t)$) or until a single flight of size larger than R is obtained (thus giving τ_e). The average time at the surface is $\tau_d = 0$. More details on the numerical simulations can be found in Appendix B. Simulations confirmed that the form of Equation (2.1) is satisfied for τ when replacing n_e by n and τ_e^0 by τ^0, where n is the average number of desorption events before the particle adsorbs at a distance r larger than R from its initial position and τ^0 is the average waiting time τ when $\tau_d = 0$.

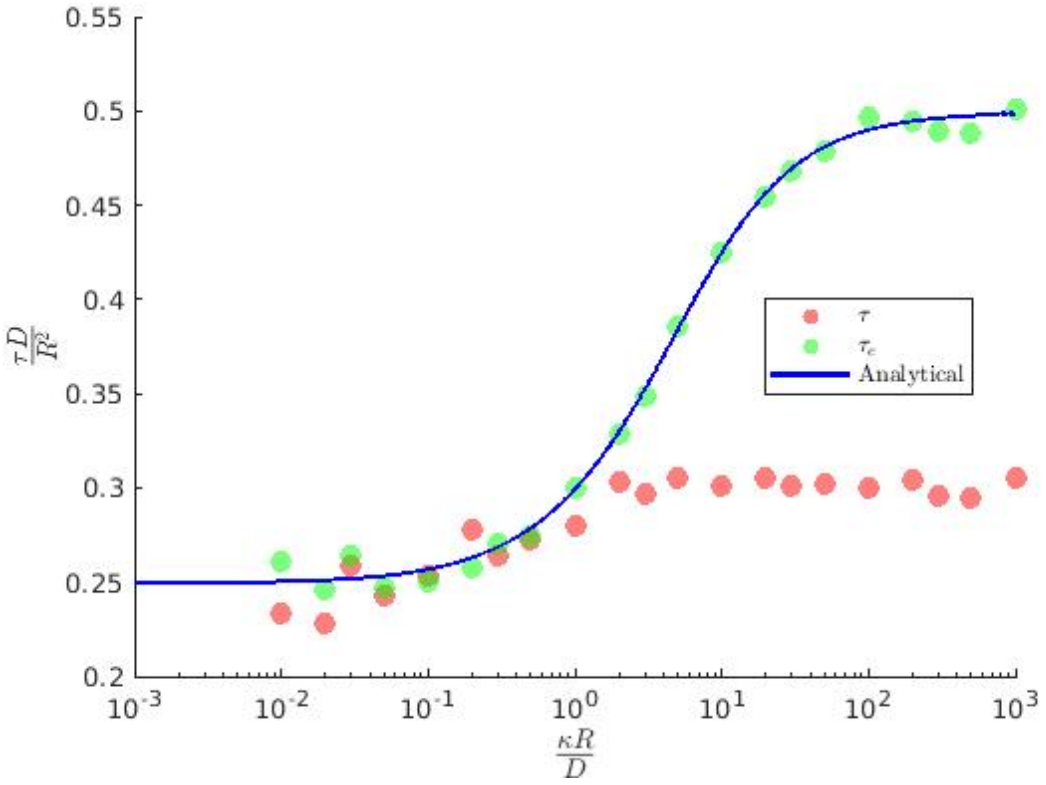

Figure 2.1: Dimensionless average waiting times from distributions ψ and ψ_e for different values of $\frac{\kappa R}{D}$, with $\tau_d = 0$. The blue line represents Equation (2.3)

.

The τ_e obtained from simulations follows the theoretical curve, as expected, see Figure 2.1. Additionally, we observe that τ is significantly smaller (by about a factor of two) compared to τ_e for $\tilde{\kappa} \gg 1$, but they become approximately equal for $\tilde{\kappa} < 1$. This is expected, since the average number of desorption events tends toward one for $\tilde{\kappa} < 1$, and the two distributions are equivalent when the particle escapes after a single desorption.

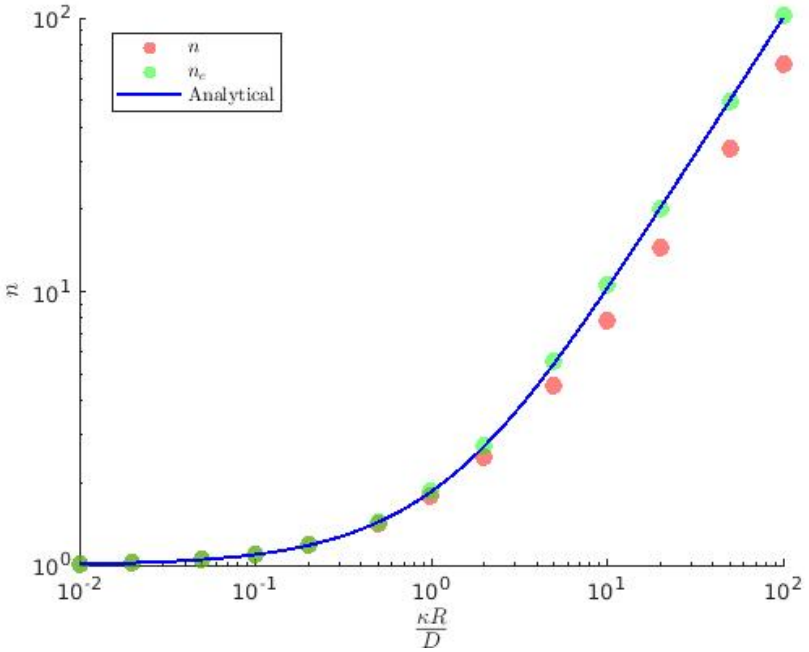

Figure 2.2: Average number of desorptions n (from the initial position) and effective number n_e (from the last desorption point) before adsorption at a distance $r > R$, as a function of $\tilde{\kappa} = \frac{\kappa R}{D}$. The blue line follows Equation (2.2).

Using the same simulation framework as for waiting times, we sampled the number of desorptions. Figure 2.2 shows that the theoretical prediction matches the simulation results for n_e. Additionally, the average number n corresponds to the analytical result for $\tilde{\kappa} < 1$, but differs (by slightly less than a factor of two) when $\tilde{\kappa} > 1$.

In conclusion, Equation (2.1) could be used to estimate the model parameters when $\tilde{\kappa} < 1$.

2.2 Tail of the PDF of apparent waiting times

In the experiments, the tail of the apparent waiting time distribution is found to decay as $t^{-5/2}$. The goal of this section is to verify whether this tail behavior can be fitted to estimate the parameters of the model.

An analytical expression for the waiting time distribution in the limit $t \to \infty$ can be obtained from Equation (1.7); see section A.3 for the detailed calculation.

$$\psi_e(t) \overset{t\to\infty}{=} c_e \; t^{-5/2} \tag{2.8}$$

where

$$c_e = \frac{R^2}{8\kappa\sqrt{\pi D}P} = \begin{cases} \frac{R^3}{8D^{3/2}\sqrt{\pi}} & \text{for } \kappa \to \infty, \\ \frac{R^2}{8\sqrt{\pi D}\kappa} & \text{for } \kappa \to 0. \end{cases} \tag{2.9}$$

Additionally, the survival probability $S_e(t) = \text{Prob}(\text{Effective desorption time} > t)$ in the long-time limit is given by:

$$S_e(t) = \frac{2}{3} c_e \; t^{-3/2}. \tag{2.10}$$

2.2.1 Numerical validation

Numerical simulations were conducted to obtain the apparent and effective waiting time distribution, as for the average waiting time. More details are given in Appendix B. The objective was to compare the tails of the distributions $\psi(t)$ and $\psi_e(t)$. The simulations were performed at $\tau_d = 0$, since the tail coefficient c_e is expected to be independent of τ_d. This assumption was tested for c and seems to be accurate for all κ.

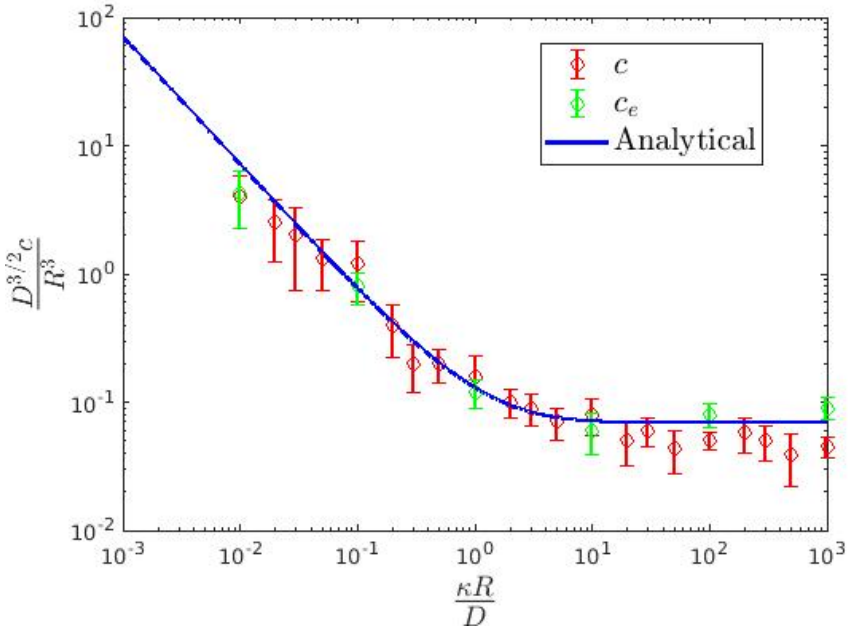

Figure 2.3: Coefficient of the adimensional tail of the apparent distribution $\tilde{c} = \frac{D^{3/2}c}{R^3}$ or effective $\tilde{c_e} = \frac{D^{3/2}c_e}{R^3}$ as a function of $\tilde{\kappa} = \frac{\kappa R}{D}$ for $\tau_d = 0$. The analytical expression for the blue line is given in Equation (2.9).

Firstly, it can be observed in Figure 2.3 that the analytical curve and the simulation data for ψ_e are in good agreement, as expected. Moreover, for $\tilde{\kappa} < 10$, the coefficients $\tilde{c}$ obtained from both ψ and ψ_e match closely, indicating that the analytical approximation is valid in this regime.

However, for $\tilde{\kappa} > 10$, the two distributions appear to be different, c is slightly below the analytical curve of about 40%.

As a consequence, it should be possible to estimate the value of $\tilde{\kappa}$ from experimental measurements of $\tilde{c_e}$ if $\tilde{\kappa} < 1$, where the analytical model remains sensitive to changes in $\tilde{\kappa}$. For larger values of $\tilde{\kappa}$, the coefficient $\tilde{c_e}$ becomes approximately constant, making the parameter estimation ineffective.

Chapter 3

Surface displacements

In this chapter we investigate the properties of the surface distribution. In what follows, we will first obtain the MSD among particles on the surface at a given time and then present analytical results for their PDF in the fast exchange limit.

3.1 Mean square displacement

The MSD $\langle x^2 \rangle_s(t)$ among particles on the surface is defined as :

$$\langle x^2 \rangle_s(t) = \frac{\int_{-\infty}^{\infty} dx \int_{-\infty}^{\infty} dy\, x^2 p_s(\underline{r}, t)}{\int_{-\infty}^{\infty} dx \int_{-\infty}^{\infty} dy\, p_s(\underline{r}, t)} = \frac{\mathcal{L}_s^{-1}[\tilde{\langle x^2 \rangle}(s)](t)}{\mathcal{L}_s^{-1}[\tilde{p_s}(\underline{k} = (0,0), s)](t)} \tag{3.1}$$

with $\mathcal{L}^{-1}$ the inverse Laplace transform operator,

$$\tilde{\langle x^2 \rangle}(s) = -\frac{\partial^2 \tilde{p_s}(\underline{k} = (k_x, k_y), s)}{\partial k_x^2}\bigg|_{k_x = k_y = 0} = \frac{D^2 \kappa k_d}{\sqrt{Ds}\left(\kappa s + D(k_d + s)\sqrt{\frac{s}{D}}\right)^2} \tag{3.2}$$

and

$$\tilde{p_s}(\underline{k} = (0,0), s) = \frac{1}{s + \frac{k_d \sqrt{Ds}}{\kappa + \sqrt{Ds}}} \tag{3.3}$$

Note that, only $\langle x^2 \rangle_s(t)$ is computed as we know that $\langle r^2 \rangle_s(t) = 2\langle x^2 \rangle_s(t)$ due to the symmetries of the surface distribution. In the next sections of this chapter, the MSD will first be characterised analytically and then be verified numerically. Finally, to try to better understand experimental results an effective diffusion constant will be defined.

3.1.1 Asymptotic Expansions and Regime Transitions

The behavior of the normalized MSD at small and large times is summarized in Table 3.1. Results are also provided in the Fast Exchange (FE) limit in which $\kappa, k_d \to \infty$ while maintaining the ratio $\delta = \kappa / k_d = O(1)$. In this limit, the Laplace expressions (3.2) and (3.3) reduce to:

$$\tilde{\langle x^2 \rangle}^{\mathrm{FE}}(s) = \frac{D^{3/2}\delta}{\sqrt{s}(\delta s + \sqrt{Ds})^2}, \quad \tilde{p}_s^{\mathrm{FE}}(\underline{k} = (0,0), s) = \frac{1}{s + \frac{\sqrt{Ds}}{\delta}}$$

The asymptotic behaviors are obtained by evaluating the Laplace transforms in the limits $s \to \infty$ (for $t \to 0$) and $s \to 0$ (for $t \to \infty$), followed by inverse Laplace transformation.

$f(t)$	$t \to 0$	$t \to \infty$
$P_s(t)$	1	$\frac{\kappa}{\sqrt{\pi D}k_d} t^{-1/2}$
$P_s^{\mathrm{FE}}(t)$	1	$\frac{\delta}{\sqrt{\pi D}} t^{-1/2}$
$\langle x^2 \rangle_s(t)$	$\frac{8\sqrt{D}\kappa k_d}{15\sqrt{\pi}} t^{5/2}$	$2Dt$
$\langle x^2 \rangle_s^{\mathrm{FE}}(t)$	$\frac{4D^{3/2}}{3\delta\sqrt{\pi}} t^{3/2}$	$2Dt$

Table 3.1: Asymptotic expansions of the MSD on the surface $\langle x^2 \rangle_s(t)$ and of the probability to be on the surface $P_s(t) = \hat{p_s}(\underline{k} = (0,0), t)$. Results in the fast exchange limit ($\kappa, k_d \to \infty$, $\kappa/k_d = \delta = O(1)$) can be identified by $^{\mathrm{FE}}$.

The short-time MSD is consistent with the expression derived in [3], in the absence of surface diffusion ($D_s = 0$).

Three distinct regimes of MSD behavior can be identified. The transition times are estimated as follows for $k_d \gg \frac{D}{\delta^2}$:

- The time $t_{5/2 \to 3/2}$ is determined by equating $\langle x^2 \rangle_s(t)$ and $\langle x^2 \rangle_s^{\mathrm{FE}}(t)$ at short times, using $\kappa = \delta k_d$.
- The time $t_{3/2 \to 1}$ is obtained from the condition $\langle x^2 \rangle_s^{\mathrm{FE}}(t \to 0) = \langle x^2 \rangle_s^{\mathrm{FE}}(t \to \infty)$.

The corresponding estimates are:

$$\begin{cases} t_{5/2 \to 3/2} = \frac{5D}{2\delta^2 k_d^2} \\ t_{3/2 \to 1} = \frac{9\pi\delta^2}{4D} \end{cases}$$

A similar calculation can be done for $k_d \ll \frac{D}{\delta^2}$. Finally the following results are obtained:

$$\langle x^2 \rangle_s(t) = \begin{cases} \frac{8\sqrt{D}\kappa k_d}{15\sqrt{\pi}} t^{5/2} & \text{for } t \lesssim \frac{D}{\delta^2 k_d^2} \\ \frac{4D^{3/2}}{3\delta\sqrt{\pi}} t^{3/2} & \text{for } \frac{D}{\delta^2 k_d^2} \lesssim t \lesssim \frac{\delta^2}{D} \\ 2Dt & \text{for } t \gtrsim \frac{\delta^2}{D} \end{cases} \quad \text{for } k_d \gg \frac{D}{\delta^2}, \tag{3.4}$$

$$\langle x^2 \rangle_s(t) = \begin{cases} \frac{8\sqrt{D}\kappa k_d}{15\sqrt{\pi}} t^{5/2} & \text{for } t \lesssim \frac{D^{1/3}}{\delta^{2/3} k_d^{4/3}} \\ 2Dt & \text{for } t \gtrsim \frac{D^{1/3}}{\delta^{2/3} k_d^{4/3}} \end{cases} \quad \text{for } k_d \ll \frac{D}{\delta^2} \tag{3.5}$$

The $t^{3/2}$ and $t^{5/2}$ regimes of the MSD had already been identified in separate papers[3, 4], but this result clarifies the conditions under which they appear. Also, the prefactor for the $t^{3/2}$ regime was not known.

3.1.2 Numerical Validation

The analytical results are validated in Figure 3.1, where the inverse Laplace transforms of Equation (3.2) and Equation (3.3) are computed numerically using the Euler inversion algorithm [1].

As expected, all three regimes are observed for $\tilde{k_d} \gg 1$, and the predicted transition times seems to agree with numerical simulations. Furthermore, in the regime $\tilde{k_d} \ll 1$, a direct transition from the $t^{5/2}$ regime to the linear regime is observed, as described in (3.5).

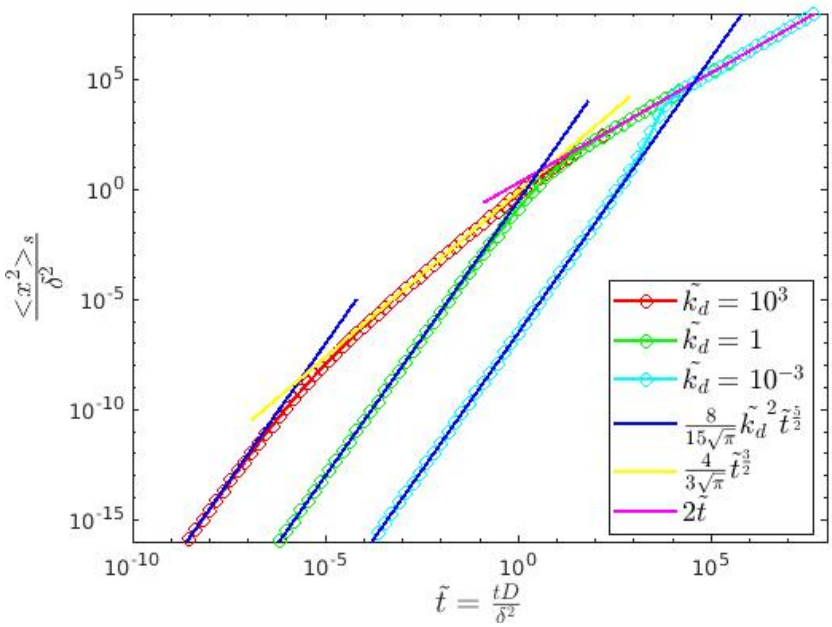

Figure 3.1: Different regimes of the MSD as a function of $\tilde{t} = \frac{Dt}{\delta^2}$ for $\tilde{k_d} = \frac{k_d\delta^2}{D}$. The dotted lines are obtained by numerically computing the inverse Laplace transform as written in Equation (3.1), while the solid lines correspond to the analytical expressions for the different regimes of the MSD.

3.1.3 Effective diffusion constant

In the experiment presented in section 1.2 a linear behaviour is obtained for the MSD to which an effective diffusion constant is associated. According to the model, when the MSD increases linearly with time the slope should be $4D$ (for $< r^2 >$), which seems to be problematic as according to the article $D > 10\,\mu m^2/s$ but the experimental effective diffusion constant (obtained by fiting the MSD) $D_{eff,exp} < 1\ \mu m^2/s$. Additionally, the surface diffusion should not explain this behaviour, as it is significantly smaller $D_s < 0.002\,\mu m^2/s$.

To try to solve this apparent inconsistency, we need to obtain an analytical expression for an effective diffusion constant that would take into account the fact that flights cannot be larger then a distance R_{max}. The exact calculation is still an ongoing work. But we guessed the expression (3.6) because with the constraint R_{max} the variance of $r = |\underline{r}|$ and the mean waiting time between two adsorptions are finite.

$$D_{eff}(R_{max}) = \frac{\langle x^2 + y^2, R_{max}\rangle}{4\langle t, R_{max}\rangle} = \frac{\int_0^\infty dtg(t)[4Dt - e^{-\frac{R_{max}^2}{4Dt}}(R_{max}^2 + 4Dt)]}{4(\frac{1}{k_d} + \int_0^\infty dtg(t)t(1 - e^{-\frac{R_{max}2}{4Dt}}))}, \tag{3.6}$$

where $\langle x^2 + y^2, R_{max}\rangle$ represents the average size of one flight which is smaller then R_{max} and $\langle t, R_{max}\rangle$ is the average waiting time between two subsequent desorptions when the flight size is smaller than R_{max}.

As it can be seen in Figure 3.2 the expression (3.6) is in good agreement with the diffusion coefficients obtained by doing simulations (and fitting the MSD with a linear curve at long time).

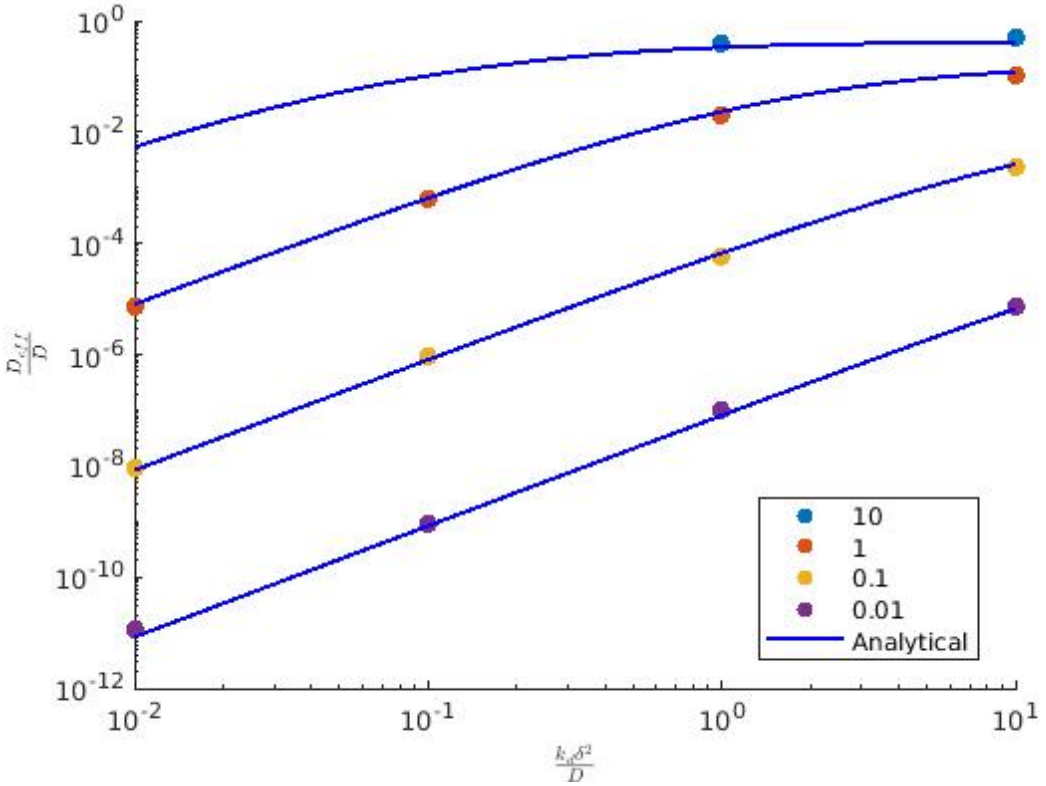

Figure 3.2: Effective diffusion constant $\tilde{D}_{eff} = \frac{D_{eff}}{D}$ as a function of $\tilde{k_d} = \frac{k_d\delta^2}{D}$ for different values of $\tilde{R}_{max} = \frac{R_{max}}{\delta}$. The numbers in the legends are the values of $\tilde{R}_{max}$ for which simulations are done. The analytical curve is given by Equation (3.6)

3.2 Non Gaussian distribution of displacement in a simplified model

In this section the goal is to predict the surface distribution of particles in the fast exchange limit (defined in subsection 3.1.1). In this case the Fourier-Laplace transform of the jump distribution, Equation (1.15), becomes:

$$\tilde{\hat{p}}_s^{\mathrm{FE}}(\underline{k}, s) = \frac{1}{s + \frac{D}{\delta}\sqrt{\underline{k}^2 + \frac{s}{D}}} \tag{3.7}$$

In order to invert the distribution numerically, an analytical expression for $\tilde{\hat{p}}_s^{\mathrm{FE}}(k,t) = \hat{p}_s^{\mathrm{FE}}(\underline{k} = (k,0), t)$ must first be obtained using the residue theorem [8]. More precisely, the poles and branch cuts of the integrand are first identified. Then, a suitable contour is defined, the residues are calculated, and partial fraction decomposition is applied to evaluate the remaining integral. The detailed calculation is given in Appendix C. The final result is :

$$\begin{aligned}\hat{P}_s^{\mathrm{FE}}(k,t) =& e^{-W_+\frac{\sqrt{D}t}{\delta}}\frac{\sqrt{1+4\delta^2k^2}-1}{\sqrt{1+4\delta^2k^2}} + \frac{e^{-Dk^2t}}{\frac{\sqrt{D}}{\delta}\sqrt{1+4\delta^2k^2}}[W_-\mathrm{erfcx}(W_-\sqrt{t}) \\ & - W_+\mathrm{erfcx}(W_+\sqrt{t})]\end{aligned} \tag{3.8}$$

with $W_\pm = \frac{\sqrt{D}}{2\delta}|1 \mp \sqrt{1+4\delta^2k^2}|$

In what follows, we will first derive asymptotic analytical expressions for the surface distribution and then verify them with numerical calculations.

3.2.1 Asymptotic analytical PDF of displacements

We could not perform the inverse Fourier transform of Equation (3.8) since e^{-Dk^2t} seemed to lead to divergences of the contour integrals. Instead, by computing $p_s(x,t) = \int_{-\infty}^{\infty} dy\, p_s(\underline{r},t)$ numerically, taking the inverse Fourier transform of Equation (3.8), it is found that the surface distribution at short time behaves as :

$$p_s^{\mathrm{FE}}(x,t) \overset{t\to 0}{=} \begin{cases} \frac{1}{t}\phi(\frac{x}{t}) & \text{for } x = O(t) \\ \psi(\frac{x}{\sqrt{t}}) & \text{for } x = O(\sqrt{t}) \end{cases} \tag{3.9}$$

and at long time, for $x = O(\sqrt{t})$:

$$p_s^{\mathrm{FE}}(x,t) \overset{t\to\infty}{=} \frac{1}{t} H(\frac{x}{\sqrt{t}}). \tag{3.10}$$

where ϕ, ψ, H are scaling functions which need to be identified.

As a consequence the following equation should be respected at short time: $\lim_{x_1=\frac{x}{t}\to\infty} \frac{1}{t}\phi(x_1) = \lim_{x_2=\frac{x}{\sqrt{t}}\to 0} \psi(x_2)$, otherwise the different regimes in Equation (3.9) do not match for $t \ll x \ll \sqrt{t}$. This leads to :

$$\begin{cases} \phi(x_1) = \frac{A}{x_1^2} & \text{for } x_1 \to \infty \\ \psi(x_2) = \frac{A}{x_2^2} & \text{for } x_2 \to 0 \end{cases}. \tag{3.11}$$

Let us first try to obtain the expression of ϕ and ψ from Equation (3.8). To do that we use the following : the $t \to 0,\ x \sim t^\alpha$ limit for the distribution can be found from the $t \to 0, k \sim t^{-\alpha}$ limit of it's Fourier transform. We proceed as follow:

$$\begin{aligned} \hat{P}_s^{\mathrm{FE}}(k = \frac{\tilde{k}}{t}, t) &= 2\int_0^\infty dx \cos(\frac{\tilde{k}}{t}x) p_s(x,t) \\ &= 2(\int_0^\epsilon dx \cos(\frac{\tilde{k}}{t}x)\frac{1}{t}\phi(\frac{x}{t}) + \int_\epsilon^\infty dx \cos(\frac{\tilde{k}}{t}x)\psi(\frac{x}{\sqrt{t}})) \end{aligned}$$

where we split the distribution $p_s(x,t)$ between the two regimes ($x = O(t)$ and $x = O(\sqrt{t})$) by introducing ϵ satisfying $t^{1/2} >> \epsilon >> t$.

Assuming the second term in the sum to give a negligible contribution in the $t \to 0$ limit

$$\hat{P}_s^{\mathrm{FE}}(k = \frac{\tilde{k}}{t}, t) \overset{x_1=\frac{x}{t}}{=} 2\int_0^{\epsilon/t} dx_1 \cos(\tilde{k}x_1)\phi(x_1)$$

The upper bound of the integral in x_1 can safely be extended to $+\infty$ when $t \to 0$ due to the expected behaviour of $\phi(\xi)$ as $x_1 \to \infty$. Thus :

$$\hat{P}_s^{\mathrm{FE}}(k = \frac{\tilde{k}}{t}, t) \overset{t\to 0}{=} \hat{\phi}(\tilde{k})$$

From the expression above ϕ can be obtained by taking the leading order of the left hand side in the $t \to 0$ limit and then doing the inverse Fourier transform. The final result is:

$$\phi(x_1) = \frac{D\delta}{\pi(D^2 + \delta^2 x_1^2)} \tag{3.12}$$

Now that the expression for ϕ has been found the expression for ψ can be obtained, in a similar manner:

$$\begin{aligned}\hat{P_s}^{\mathrm{FE}}(k=\frac{\tilde{k}}{\sqrt{t}},t) &= 2(\int_0^{\epsilon} dx\cos(\frac{\tilde{k}}{\sqrt{t}}x)\frac{1}{t}\phi(\frac{x}{t})+\int_{\epsilon}^{\infty} dx\cos(\frac{\tilde{k}}{\sqrt{t}}x)\psi(\frac{x}{\sqrt{t}}))\\ &= 2\{\int_0^{\infty} dx\cos(\frac{\tilde{k}}{\sqrt{t}}x)\frac{1}{t}\phi(\frac{x}{t})+\int_{\epsilon}^{\infty} dx\cos(\frac{\tilde{k}}{\sqrt{t}}x)[\psi(\frac{x}{\sqrt{t}})-\frac{1}{t}\phi(\frac{x}{t})]\}\end{aligned}$$

where we used $\int_0^{\epsilon} dx\cos(\frac{\tilde{k}}{\sqrt{t}}x)\frac{1}{t}\phi(\frac{x}{t}) = \int_0^{\infty} dx\cos(\frac{\tilde{k}}{\sqrt{t}}x)\frac{1}{t}\phi(\frac{x}{t}) - \int_{\epsilon}^{\infty} dx\cos(\frac{\tilde{k}}{\sqrt{t}}x)\frac{1}{t}\phi(\frac{x}{t})$.
Now by taking $x_1 = \frac{x}{t}$, $x_2 = \frac{x}{\sqrt{t}}$ we get:

$$\hat{P_s}^{\mathrm{FE}}(k=\frac{\tilde{k}}{\sqrt{t}},t) = 2\{\int_0^{\infty} dx_1\cos(\tilde{k}x_1\sqrt{t})\phi(x_1)+\int_{\epsilon/\sqrt{t}}^{\infty} dx_2\sqrt{t}\cos(\tilde{k}x_2)[\psi(x_2)-\frac{1}{t}\phi(\frac{x_2}{\sqrt{t}})]\}$$

By taking the $t\to 0$ limit $\phi(\frac{x_2}{\sqrt{t}}) = \frac{At}{x_2^2}$ and thus the lower bound of the second integral can be safely set to 0. So the following equation is obtained:

$$\hat{P_s}^{\mathrm{FE}}(k=\frac{\tilde{k}}{\sqrt{t}},t) = 1-|\tilde{k}|\sqrt{t}+\sqrt{t}\hat{G}(\tilde{k}),$$

where $G(x_2) = \psi(x_2) - \frac{A}{x_2^2}$ and $\hat{\phi}(\tilde{k}\sqrt{t}) = 1-|\tilde{k}|\sqrt{t}+O(t)$ are used. By expanding the equation above in the $t\to 0$ limit we get an equation for $\hat{G}(\tilde{k})$ from wich ψ can be obtained:

$$\psi(x_2) = \frac{D\ e^{-\frac{x_2^2}{4D}}}{\pi\delta x_2^2} - \frac{\Gamma(0,\frac{x_2^2}{4D})}{4\pi\delta} \tag{3.13}$$

where $\Gamma(0,x) = \int_x^{\infty} dt\frac{e^{-t}}{t}$.

Now that we obtained ϕ and ψ, let us obtain H, as follow :

$$p_s^{\mathrm{FE}}(x=x_2\sqrt{t},t) = \frac{1}{2\pi}\int_{-\infty}^{\infty} dk\ \cos(k\,x_2\sqrt{t})\,\hat{p}_s(k,t) \tag{3.14}$$

$$\overset{\tilde{k}=kx_2\sqrt{t}}{=} \frac{1}{\pi x_2\sqrt{t}}\int_0^{\infty} d\tilde{k}\ \cos(\tilde{k})\,\hat{p}_s(\frac{\tilde{k}}{x_2\sqrt{t}},t) \tag{3.15}$$

Then, by keeping only the leading order of the long time expansion of $\hat{p}_s(\frac{\tilde{k}}{x_2\sqrt{t}},t)$ the integral can be computed. Which allows us to obtain:

$$H(x_2) = \frac{\delta e^{-\frac{x_2^2}{4D}}}{2\pi D} \tag{3.16}$$

Note that the constraints of Equation (3.11) are satisfied and that $A = \frac{D}{\pi\delta}$. Moreover, the normalised distribution on the surface, in the long time limit, for $x = O(\sqrt{t})$, can be deduced from $H(x_2)$ and is Gaussian :

$$p_s^{\mathrm{FE,N}}(t,x) = \frac{p_s^{\mathrm{FE}}(t,x)}{P_s(t)} \overset{t\to\infty}{=} \mathcal{N}(0,\,2Dt) \tag{3.17}$$

where $P_s(t)$ is the probability to be on the surface (given for $t\to\infty$ in Table 3.1) and $\mathcal{N}(0,\,2Dt) = \frac{e^{-\frac{x^2}{4Dt}}}{\sqrt{4\pi Dt}}$.

3.2.2 Numerical Validation

Now that the distribution has been characterised analytically in three different regimes let's compare them to numerical calculations. The surface distribution is obtained numerically by using fast Fourier transform on Equation (3.8).

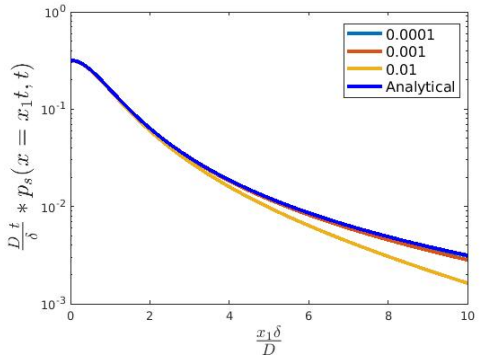

(a)

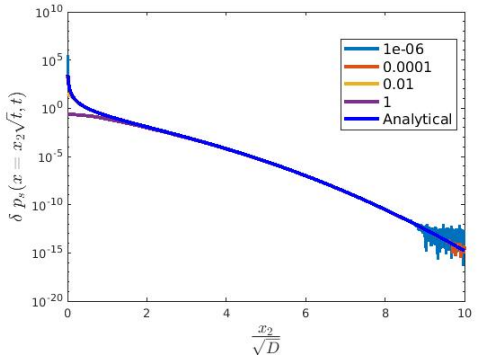

(b)

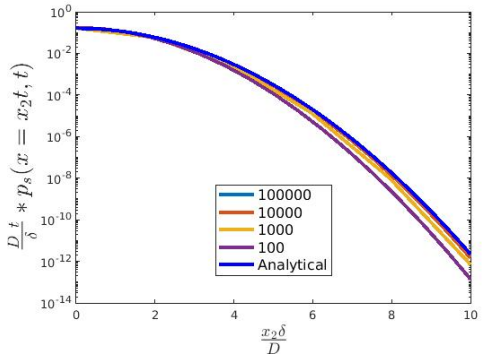

(c)

Figure 3.3: Surface distribution of particles at short time for (a) $x = O(t)$, (b) $x = O(\sqrt{t})$ and (c) at long time with $x = O(\sqrt{t})$. The analytical curves in (a), (b) and (c) are given respectively by the adimensionalised Equation (3.12), (3.13)and (3.16). The numbers in the legends are the values of $\tilde{t} = \frac{Dt}{\delta^2}$ for which the distribution is evaluated, by numerically computing the inverse Fourier transform of Equation (3.8).

As can be seen in Figure 3.3 the analytical expressions obtained for the distributions $\phi(\frac{x}{t})$, $\psi(\frac{x}{\sqrt{t}})$ and $H(\frac{x}{\sqrt{t}})$ are in very good agreement with the numerical results. The fact that the blue points are spread in Figure 3.3(a) is due to the numerical errors arising for large x_2 and short t.

So, the behaviour of the surface distribution, in the fast exchange limit has been characterised at short time for two different regimes and at long time in one regime.

Chapter 4

Conclusion

In the introduction, we stated that the experimental results showing Bulk mediated surface displacements were poorly understood by the theory. For this reason, in this work we tried to provide explanations for the experimental results, using the simplest model for BMSD.

First, we tried to provide a method for extracting the parameters of the model from the average and the tail distribution of the apparent waiting times. From numerical simulations, it appears that the parameters can be estimated when $\tilde{\kappa} < 1$, as the analytical approximation we obtained is valid only in this regime.

Then, the MSD was characterized in different regimes, depending on time and the desorption rate k_d. The results suggest that the different time scalings of the MSD, already predicted by theoretical arguments at short times, could correspond to different regimes of k_d. Moreover, we presented a first attempt to explain the effective MSD observed in experiments.

Finally, we characterized the surface distributions in the fast exchange limit, at both short and long times. At short times, the distribution is non-Gaussian, both in its peak and its tail. However, at long times, the normalized surface PDF becomes Gaussian.

To conclude this report, our results suggest that the model we used can provide a qualitative explanation for the experimental observations. However, to achieve a quantitative explanation, further work is needed: first, to derive an analytical expression for the effective MSD (or diffusion constant), and then to fit the two model parameters (κ and k_d) to the apparent waiting time distribution (for example), and finally to check whether the predicted effective diffusion constant is correct. Lastly, it would be interesting to obtain the general surface distribution without taking the fast exchange limit.

References

[1] Joseph Abate and Ward Whitt. "A Unified Framework for Numerically Inverting Laplace Transforms". In: *INFORMS J. on Computing* 18.4 (Jan. 2006), pp. 408–421. ISSN: 1526-5528.

[2] A. Alexandre et al. "How Stickiness Can Speed Up Diffusion in Confined Systems". In: *Phys. Rev. Lett.* 128 (21 May 2022), p. 210601.

[3] Alexander M. Berezhkovskii, Leonardo Dagdug, and Sergey M. Bezrukov. "A new approach to the problem of bulk-mediated surface diffusion". In: *The Journal of Chemical Physics* 143.8 (Aug. 2015), p. 084103.

[4] Oleg V. Bychuk and Ben O'Shaughnessy. "Anomalous Diffusion at Liquid Surfaces". In: *Phys. Rev. Lett.* 74 (10 Mar. 1995), pp. 1795–1798.

[5] T. Calandre, O. Bénichou, and R. Voituriez. "Accelerating search kinetics by following boundaries". In: *Phys. Rev. Lett.* 112 (23 June 2014), p. 230601.

[6] Shlomo Havlin and Daniel Ben-Avraham and. "Diffusion in disordered media". In: *Advances in Physics* 36.6 (1987), pp. 695–798.

[7] Felix Höfling and Thomas Franosch. "Anomalous transport in the crowded world of biological cells". In: *Reports on Progress in Physics* 76.4 (Mar. 2013), p. 046602.

[8] John M. Howie. *Complex Analysis*. Springer, 2003.

[9] Katja Lindenberg, Ralf Metzler, and Gleb Oshanin. *Chemical Kinetics: Beyond the Textbook*. WORLD SCIENTIFIC (EUROPE), Dec. 2018.

[10] Paolo Malgaretti, Ignacio Pagonabarraga, and Miguel Rubi. "Entropic transport in confined media: a challenge for computational studies in biological and soft-matter systems". In: *Frontiers in Physics* Volume 1 - 2013 (2013).

[11] Michael J. Skaug, Joshua Mabry, and Daniel K. Schwartz. "Intermittent Molecular Hopping at the Solid-Liquid Interface". In: *Phys. Rev. Lett.* 110 (25 June 2013), p. 256101.

[12] Michael J. Skaug, Joshua N. Mabry, and Daniel K. Schwartz. "Single-Molecule Tracking of Polymer Surface Diffusion". In: *Journal of the American Chemical Society* 136.4 (2014), pp. 1327–1332.

[13] Daniel Tartakovsky and Marco Dentz. "Diffusion in Porous Media: Phenomena and Mechanisms". In: *Transport in Porous Media* 130 (Oct. 2019), pp. 1–23.

[14] Dapeng Wang and Daniel K. Schwartz. "Non-Brownian Interfacial Diffusion: Flying, Hopping, and Crawling". In: *The Journal of Physical Chemistry C* 124.37 (2020), pp. 19880–19891.

[15] Dapeng Wang, Haichao Wu, and Daniel K. Schwartz. "Three-Dimensional Tracking of Interfacial Hopping Diffusion". In: *Phys. Rev. Lett.* 119 (26 Dec. 2017), p. 268001.

[16] Changqian Yu et al. “Single-Molecule Observation of Long Jumps in Polymer Adsorption”. In: *ACS Nano* 7.11 (2013), pp. 9735–9742.

Appendix A

Preliminary calculations

In this chapter of the Appendix, preliminary computations, that had been obtained before the internship, are presented.

A.1 Derivation of the waiting time distribution for bulk diffusion

The distribution of waiting time $g(t)$ to readsorb after a desorption is computed, in the followi. To obtain g, we consider $p(z,t)$ the PDF of z for particles that have not been absorbed at t, which satisfies Equation (1.3)–(1.5). Taking the Laplace transform of Equation (1.3) with respect to the position z, with u the name of the Laplace variable, we obtain

$$\partial_t \tilde{p}(u,t) = D[u^2 \tilde{p}(u,t) - \partial_z p(0,t) - u\ p(0,t)]. \tag{A.1}$$

Then the boundary condition (1.5) is used :

$$\partial_t \tilde{p}(u,t) = Du^2 \tilde{p}(u,t) - \kappa\ p_0(t) - Du\ p_0(t) \tag{A.2}$$

where we have defined $p_0(t) = p(z=0,t)$. Now we take the Laplace transform with respect to the variable t, with s the name of the Laplace variable:

$$s\tilde{\tilde{p}}(u,s) - 1 = Du^2 \tilde{\tilde{p}}(u,s) - \kappa\ \tilde{p}_0(s) - Du\tilde{p}_0(s). \tag{A.3}$$

Since $p(z,t)$ decays at long z, its Laplace transform must be finite for all u. Therefore, writing the above equation for $s = Du^2$ leads to

$$\tilde{p}_0(s) = \frac{1}{\kappa + \sqrt{sD}}. \tag{A.4}$$

Inserting this value back into Eq. (A.3) leads to

$$\tilde{\tilde{p}}(u,s) = \frac{\sqrt{D}}{(\sqrt{s} + \sqrt{D}u)(\kappa + \sqrt{sD})}. \tag{A.5}$$

The probability that the particle is not adsorbed at t is $S(t) = \int_0^\infty dz p(z,t) = \tilde{p}(u=0,t)$, so that with $g(t) = -\partial_t S$, we have

$$\tilde{g}(s) = 1 - s\ \tilde{\tilde{p}}(u=0,s) = \frac{\kappa}{\kappa + \sqrt{sD}}. \tag{A.6}$$

Inverting the Laplace transform leads to an analytical expression for the distribution of adsorption times, right after a desorption event:

$$g(t) = \frac{\kappa^2}{D}\left[\frac{\sqrt{D}}{\sqrt{\pi\ t\ \kappa^2}} - \mathrm{erfcx}\left(\sqrt{\frac{\kappa^2 t}{D}}\right)\right], \tag{A.7}$$

A.2 Computation of the Laplace transform of the effective waiting time distribution

In the following, the Laplace transform of the effective waiting time distribution is obtained. Consider a scenario where a random walk has a probability P to end at each flight. Then let us call p_n the probability that the escape occurs at the n^{th} flight, with $n \geq 1$. In this case

$$p_n = (1-P)^{n-1}P \tag{A.8}$$

Now, let us call $p(t)$ the probability that a jump starting from the origin lasts a time t given that it does not escape out of the disk, hence

$$\begin{aligned} p(t) &= \frac{g(t)}{1-P}\int_{|\underline{r}|<R} d\underline{r}\ \frac{e^{-\underline{r}^2/(4Dt)}}{4\pi Dt} = \frac{g(t)}{1-P}2\pi\int_0^R dr\ r\ \frac{e^{-r^2/(4Dt)}}{4\pi Dt} \\ &= \frac{g(t)}{1-P}\left(1-e^{-R^2/(4Dt)}\right). \end{aligned} \tag{A.9}$$

Now, consider $p^*(t)$ the probability density that the sum of the detachment time and of the jump time given that the size of the flight is less than R:

$$p^*(t) = \int_0^t dt'\psi_d(t')p(t-t') \tag{A.10}$$

with $\psi_d(t) = e^{-k_d t}k_d$ the distribution of desorption times. Call $F_n(T)$ the distribution of the time before the last flight, given that the escape occurs at the flight number n. Then

$$F_1(T) = \psi_d(T), \tag{A.11}$$

$$F_n(T) = \int dt_1 dt_2 ....dt_n \psi_d(t_1)p^*(t_2)....p^*(t_n)\delta(T - t_1 - t_2.... - t_n) \qquad (n \geq 2) \tag{A.12}$$

Hence, taking the temporal Laplace transform leads to

$$\tilde{F}_n(s) = \tilde{\psi}_d(s)[\tilde{p}^*(s)]^{n-1} = [\tilde{\psi}_d(s)]^n[\tilde{p}(s)]^{n-1} \qquad (n \geq 1) \tag{A.13}$$

Then the distribution of the time elapsed before the last flight is

$$\psi_e(T) = \sum_{n=1}^{\infty} p_n F_n(T), \tag{A.14}$$

so that

$$\tilde{\psi}_e(s) = \sum_{n=1}^{\infty}(1-P)^{n-1}P[\tilde{\psi}_d(s)]^n[\tilde{p}(s)]^{n-1} \tag{A.15}$$

and thus

$$\tilde{\psi}_e(s) = \frac{P\tilde{\psi}_d(s)}{1-(1-P)\tilde{\psi}_d(s)\tilde{p}(s)} \tag{A.16}$$

A.3 Analytical calculation of the tail of the effective waiting time distribution

The waiting time distribution $\psi_e(t)$ in the limit of $t \to \infty$ can be obtained from Equation (1.7). First, $\tilde{p}(s)$ has to be evaluated as $s \to 0$:

$$\tilde{p}(s) = \int_0^\infty dt e^{-st} \frac{g(t)}{1-P}(1 - e^{-\frac{R^2}{4Dt}}) = 1 - \tau_b^p s + \int_0^\infty dt (e^{-st} - 1 + ts) \frac{g(t)}{1-P}(1 - e^{-\frac{R^2}{4Dt}}) \tag{A.17}$$

$$\stackrel{u=st}{=} 1 - \tau_b^p s + \int_0^\infty \frac{du}{s}(e^{-u} - 1 + u) \frac{g(u/s)}{1-P}(1 - e^{-\frac{R^2}{4D(u/s)}}) \tag{A.18}$$

$$\stackrel{s\to 0}{=} 1 - \tau_b^p s + \frac{R^2}{6(1-P)\kappa\sqrt{D}} s^{3/2} + O(s^2) \tag{A.19}$$

Where $\tau_b^p = \int_0^\infty dt\, t \frac{g(t)}{1-P}(1 - e^{-\frac{R^2}{4Dt}})$ the expression $g(t) \stackrel{t\to\infty}{=} \frac{\sqrt{D}}{2t^{3/2}\kappa\sqrt{\pi}}$ is used. Moreover, we know that $\tilde{\psi_d}(s) = \frac{k_d}{k_d+s}$.

Thus we can expand $\tilde{\psi_e}(s)$ at $s \to 0$:

$$\tilde{\psi_e}(s) = \frac{P\tilde{\psi_d}(s)}{1 - (1-P)\tilde{\psi_d}(s)\tilde{p}(s)} \stackrel{s\to 0}{=} 1 - \tau_e s + \frac{R^2}{6\kappa\sqrt{D}P} s^{3/2} + O(s^2). \tag{A.20}$$

Combining the following equation

$$\int_0^\infty dt\, \psi_e(t)(e^{-st} - 1 + st) \stackrel{t'=st}{=} \int_0^\infty \frac{dt'}{s}\, \psi_e(\frac{t'}{s})(e^{-t'} - 1 + t') \tag{A.21}$$

with the anzatz $\psi_e(t) \stackrel{t\to\infty}{=} c_e t^{-5/2}$ and taking the limit $s \to 0$, we obtain :

$$\int_0^\infty dt' \frac{c_e\, s^{3/2}}{t'^{5/2}}(e^{-t'} - 1 + t') = \frac{R^2}{6\kappa\sqrt{D}P} s^{3/2}. \tag{A.22}$$

After computing the integral, the coefficient c_e is found. Finally the tail of the distribution is given by :

$$\psi_e(t) \stackrel{t\to\infty}{=} c_e\ t^{-5/2}.$$

where $c_e = \frac{R^2}{8\kappa\sqrt{\pi D}P}$

A.4 Computation of Fourier-Laplace transform of the surface distribution

In the following the Fourier-Laplace transform of the surface distribution is obtained from Equation (1.10)–(1.14).

We first take the Laplace transform in position z (with u the Laplace variable) we obtain

$$\partial_t \tilde{p}_b(\underline{r}, u, t|\sigma) = D(u^2 + \nabla_{\underline{r}}^2)\tilde{p}_b(\underline{r}, u, t|\sigma) - D\partial_z p_b(\underline{r}, 0, t|\sigma) - Dup_b(\underline{r}, 0, t|\sigma)] \tag{A.23}$$

which can also be written

$$\partial_t \tilde{p}_b(\underline{r}, u, t|\sigma) = D(u^2 + \nabla_{\underline{r}}^2)\tilde{p}_b(\underline{r}, u, t|\sigma) - \kappa\ p_0(\underline{r}, t|\sigma) - Dup_0(\underline{r}, t|\sigma) + k_d p_s(\underline{r}, t|\sigma) \tag{A.24}$$

where we have defined $p_0(\underline{r}, t|\sigma) = p_b(\underline{r}, z = 0, t|\sigma)$. Now we take the Laplace transform for the variable t with s the name of the Laplace variable, and the Fourier transform of $\underline{r}$ with $\underline{k}$ the name of the Fourier variable

$$s\tilde{\hat{p}}_b(\underline{k}, u, s|\sigma) = D(u^2 - \underline{k}^2)\tilde{\hat{p}}_b(\underline{k}, u, s|\sigma) - \kappa\ \tilde{\hat{p}}_0(\underline{k}, s|\sigma) - Du\tilde{\hat{p}}_0(\underline{k}, s|\sigma) + k_d\tilde{\hat{p}}_s(\underline{k}, s|\sigma) \tag{A.25}$$

$$s\tilde{\hat{p}}_s(\underline{k}, s|\sigma) - 1 = \kappa\ \tilde{\hat{p}}_0(\underline{k}, s|\sigma) - k_d\tilde{\hat{p}}_s(\underline{k}, s|\sigma) \tag{A.26}$$

Since $\tilde{\hat{p}}_b(\underline{k}, u, s)$ cannot be infinite for any value of u (because it does not diverge for large z), applying the above equation for $u = \sqrt{\underline{k}^2 + s/D}$ leads to

$$-\kappa\ \tilde{\hat{p}}_0(\underline{k}, s|\sigma) - D\sqrt{\underline{k}^2 + \frac{s}{D}}\tilde{\hat{p}}_0(\underline{k}, s|\sigma) + k_d\tilde{\hat{p}}_s(\underline{k}, s|\sigma) = 0 \tag{A.27}$$

so that

$$\tilde{\hat{p}}_0(\underline{k}, s|\sigma) = \frac{k_d}{\kappa + D\sqrt{\underline{k}^2 + \frac{s}{D}}}\tilde{\hat{p}}_s(\underline{k}, s|\sigma). \tag{A.28}$$

Using Eq. (A.26) we get :

$$(s + k_d)\tilde{\hat{p}}_s(\underline{k}, s|\sigma) - 1 = \frac{\kappa k_d}{\kappa + D\sqrt{\underline{k}^2 + \frac{s}{D}}}\tilde{\hat{p}}_s(\underline{k}, s) \tag{A.29}$$

so that

$$\tilde{\hat{p}}_s(\underline{k}, s|\sigma) = \frac{1}{s + k_d - \frac{\kappa k_d}{\kappa + D\sqrt{\underline{k}^2 + \frac{s}{D}}}} = \frac{1}{s + \frac{k_d D\sqrt{\underline{k}^2 + \frac{s}{D}}}{\kappa + D\sqrt{\underline{k}^2 + \frac{s}{D}}}}. \tag{A.30}$$

Appendix B

Numerical simulations

During the internship, numerical simulations were done by generating random numbers from $\psi_d(t)$, $g(t)$ and Gaussian distributions. It can be done using the equality

$$X = \mathrm{CDF}_q^{-1}(U) \tag{B.1}$$

where U, X are random variables respectively distributed according to a uniform distribution between 0 and 1 and $q(x)$. Moreover, CDF_q^{-1} is the inverse Cumulative Distribution Function (CDF) of $q(x)$ (distribution from which we want to generate samples).

Using Equation (B.1), waiting times t from $\psi_d(t)$ are generated as follow : $t = -\frac{1}{k_d} \ln U$. But for $t' \sim g(t')$ since the inverse CDF of $g(t)$ cannot be obtained analytically, samples are obtained by finding the time t' such that $U - \mathrm{CDF}_g(t) = 0$ numerically.

Finally, random variables can be generated from more complex distribution such as $\psi(t)$ and $\psi_e(t)$ as described in Algorithm 1 and 2

Algorithm 1 $\psi(t)$

function $\psi(\kappa, R, D, \tau_d)$
  $x \leftarrow 0$; $y \leftarrow 0$
  $t_\psi \leftarrow 0$;
  while $\sqrt{x^2 + y^2} < R$ **do**
    $t_d \sim \psi_d(t \mid \tau_d)$
    $t_\psi \leftarrow t_\psi + t_d + t_g$
    $t_g \sim g(t \mid \kappa, D)$
    $x \leftarrow x + \mathcal{N}(0, 2Dt_g)$
    $y \leftarrow y + \mathcal{N}(0, 2Dt_g)$
  end while
  return t_ψ
end function

Algorithm 2 $\psi_e(t)$

function $\psi_e(\kappa, R, D, \tau_d)$
  $t_{\psi_e} \leftarrow 0$
  while $\sqrt{x^2 + y^2} < R$ **do**
    $t_d \sim \psi_d(t \mid \tau_d)$
    $t_{\psi_e} \leftarrow t_{\psi_e} + t_d + t_g$
    $t_g \sim g(t \mid \kappa, D)$
    $x \sim \mathcal{N}(0, 2Dt_g)$
    $y \sim \mathcal{N}(0, 2Dt_g)$
  end while
  return t_{ψ_e}
end function

Appendix C

Inverse Laplace transform of the surface distribution in the FE limit

In this section the inverse Laplace transform of Equation (3.7) is computed, but first branch cuts are defined.

To make multi-valued functions single-valued branch cuts, in which a function is not defined needs, need to be introduced . An example of such a function would be

$$\sqrt{z} = \sqrt{re^{i\theta}} = r^{\frac{1}{2}} e^{i\frac{\theta}{2}}$$

since for $z \in \mathbb{C}$ there are two possible values of $\sqrt{z}$: $r^{\frac{1}{2}} e^{i\frac{\theta}{2}}$ and $r^{\frac{1}{2}} e^{i\frac{\theta}{2}+\pi}$.

From now on the adimensional version of Equation (3.7) (equivalent to taking $D = \delta = 1$) is used.

$$\tilde{\hat{p}}_s^{\mathrm{FE}}(k,s) = \frac{1}{s+\sqrt{k^2+s}}. \tag{C.1}$$

The inverse Laplace transform of Equation (C.1) can be writen as :

$$\hat{p_s}^{simp}(k,t) = \int_{L-i\infty}^{L+i\infty} ds \frac{e^{st}}{2\pi i} \frac{1}{s+\sqrt{k^2+s}} \tag{C.2}$$

where $L \in \mathbb{R}$ is larger than the real part of all the singularities of $f(s) = \frac{e^{st}}{2\pi i} \frac{1}{s+\sqrt{k^2+s}}$. We can notice that $f(s)$ has one branch point in $k^2 + s_{branch} = 0 \iff s_{branch} = -k^2$, we will choose the branch cut such that $-\pi < \arg(k^2+s) < \pi$. Moreover, the function has one pole which can be found by solving $s^2 = k^2 + s$ which gives $s_\pm = \frac{1\pm\sqrt{1+4k^2}}{2}$ but it can be checked that the only pole is $s_- = \frac{1-\sqrt{1+4k^2}}{2}$.

Based on the position of the branch point and of the pole, we choose to define the integration contour as illustrated in Figure C.1.

Using the residue theorem [8] we can write :

$$\hat{p}_s^{\mathrm{FE}}(k,t) = \int_{c_1} ds\, f(s) = 2\pi i \,\mathrm{Res}(f, s_-) - \int_{c_2+c_3+c_4+c_5+c_6} ds\, f(s) \tag{C.3}$$

Let us try to show that the c_2, c_4 and c_6 integrals are equal to 0 :

$$\left| \int_{c_2} ds f(s) \right| \overset{s=Re^{i\theta}+L}{=} \left| \int_{c_2} d\theta f'(\theta) \right| \leq \int_{\pi/2}^{\pi} d\theta \left| R\ i\ e^{i\theta} \frac{e^{(Re^{i\theta}+L)t}}{2\pi i} \frac{1}{Re^{i\theta}+L+\sqrt{k^2+Re^{i\theta}+L}} \right|$$

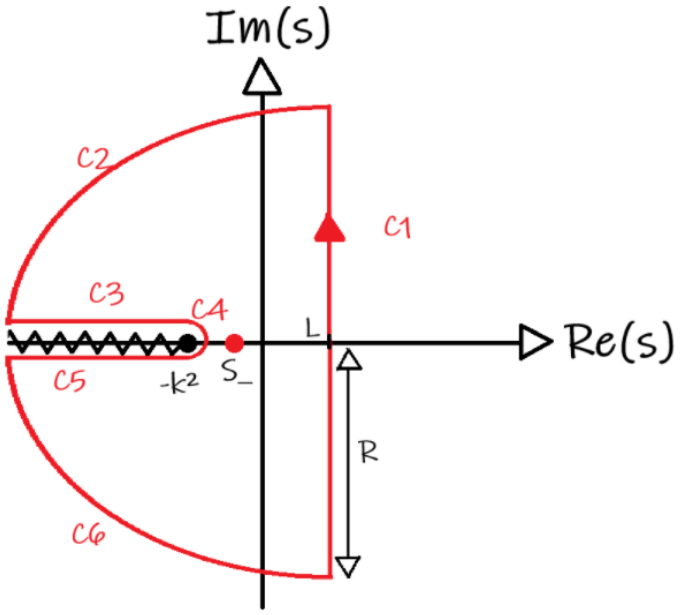

Figure C.1: Contour integration used to obtain the inverse Laplace transform of Equation (C.1). The contour is divided in different parts called c_1 to c_6, it contains the pole s_- and doesn't cross the branch cut (located between $s = -k^2$ and $s = -\infty$). The circle arcs c_2 and c_6 are at a distance R from the center located in $s = L$.

$$\overset{R\to\infty}{=} \int_{\pi/2}^{\pi} d\theta R \frac{e^{(R\cos(\theta)+L)t}}{2\pi}\frac{1}{R} = \frac{e^{Lt}}{2\pi}\int_{\pi/2}^{\pi} d\theta e^{R\cos(\theta)t} = 0$$

for finite t, where $f'(\theta) = f(s = Re^{i\theta} + L)$ and $|Re^{i\theta} + L + \sqrt{k^2 + Re^{i\theta} + L}| \overset{R\to\infty}{\to} R$ are used. Similarly $|\int_{c_6} ds f(s)| = 0$. Now for c_4 :

$$\begin{aligned}
|\int_{c_4} ds\, f(s)| &\overset{s=re^{i\theta}-k^2}{=} |\int_{c_4} d\theta f'(\theta)| \leq \int_{c_4} d\theta |f'(\theta)| \\
&\leq \int_{\pi/2}^{-\pi/2} d\theta\ |r\ i\ e^{i\theta}\frac{e^{(re^{i\theta}-k^2)t}}{2\pi i}\frac{1}{re^{i\theta} - k^2 + \sqrt{k^2 + re^{i\theta} - k^2}}| \\
&\overset{r\to 0}{\leq} \frac{re^{-k^2t}}{2\pi k^2}\int_{\pi/2}^{-\pi/2} d\theta e^{r\cos(\theta)t} = 0.
\end{aligned}$$

Note that it is also equal to 0 when $k = 0$.

Thus we only have to evaluate the c_3 and c_5 integrals. Let's first evaluate the c_3 integral :

$$\begin{aligned}
\int_{c_3} f(s)ds &= \int_{-\infty}^{-k^2} ds \frac{e^{st}}{2\pi i}\frac{1}{s + \sqrt{k^2 + s}} = \int_{-\infty}^{-k^2} ds \frac{e^{st}}{2\pi i}\frac{1}{s + \sqrt{|k^2 + s|}\ i} \\
&\overset{u=s+k^2}{=} \frac{1}{2\pi i}\int_{-\infty}^{0} du \frac{e^{-k^2t}e^{ut}}{u - k^2 + i|u|^{1/2}} \overset{v=-u}{=} \frac{1}{2\pi i}\int_{0}^{\infty} dv \frac{e^{-k^2t}e^{-vt}}{-v - k^2 + iv^{1/2}}.
\end{aligned}$$

Similarly, with the appropriate phase and bounds the c_5 integral gives :

$$\int_{c_5} f(s)ds = -\frac{1}{2\pi i}\int_{0}^{\infty} dv \frac{e^{-k^2t}e^{-vt}}{-v - k^2 - iv^{1/2}}.$$

Thus :

$$\int_{c_3+c_5} dsf(s) = -\frac{e^{-k^2t}}{\pi}\int_0^\infty dV \frac{e^{-Vt}\sqrt{V}}{(V+k^2)^2+V}.$$

Partial fraction decomposition is used :

$$\frac{1}{(V+k^2)^2+V} = \frac{1}{\sqrt{1+4k^2}}\left(\frac{1}{V-V_+} - \frac{1}{V-V_-}\right) \tag{C.4}$$

where $V_\pm = -(\frac{1\mp\sqrt{1+4k^2}}{2})^2$.

This last simplification permits the computation of the integral :

$$\int_{c_3+c_5} dsf(s) = -\frac{e^{-k^2t}}{\sqrt{1+4k^2}}\left(\sqrt{-V_-}\text{erfcx}(\sqrt{-V_-t}) - \sqrt{-V_+}\text{erfcx}(\sqrt{-V_+t})\right) \tag{C.5}$$

Now the residue is evaluated, since the pole is inside the integration contour. To do so we use the following theorem [8] : given a function $f(z) = \frac{g(z)}{h(z)}$, where g and h are both holomorphic in a neighbourhood of c, and where $h(c) = 0$, $h'(c) \neq 0$. Then

$$\text{Res}(f, c) = \frac{g(c)}{h'(c)}.$$

We already know $h(s_-) = s_- + \sqrt{k^2+s_-} = 0$. $h'(s_-) = 1 + \frac{1}{2\sqrt{k^2+s_-}} = \frac{\sqrt{1+4k^2}}{\sqrt{1+4k^2}-1} \neq 0\ \forall k \in \mathbb{R}$. Thus we get $\text{Res}(f, s_-) = \frac{e^{\frac{1-\sqrt{1+4k^2}}{2}t}}{2\pi i}\frac{\sqrt{1+4k^2}-1}{\sqrt{1+4k^2}}$

Finally, Equation (C.3) becomes :

$$\hat{P}_s^{\text{FE}}(k,t) = e^{-\sqrt{-V_+}\,t}\frac{\sqrt{1+4k^2}-1}{\sqrt{1+4k^2}} + \frac{e^{-k^2t}}{\sqrt{1+4k^2}}\left(\sqrt{-V_-}\text{erfcx}(\sqrt{-V_-t}) - \sqrt{-V_+}\text{erfcx}(\sqrt{-V_+t})\right).$$

Putting dimensions back into the equation and simplifying the notation :

$$\begin{aligned}\hat{P}_s^{\text{FE}}(k,t) =& e^{-W_+\frac{\sqrt{D}\,t}{\delta}}\frac{\sqrt{1+4\delta^2k^2}-1}{\sqrt{1+4\delta^2k^2}} + \frac{e^{-Dk^2t}}{\frac{\sqrt{D}}{\delta}\sqrt{1+4\delta^2k^2}}\left(W_-\text{erfcx}(W_-\sqrt{t})\right.\\ &\left. - W_+\text{erfcx}(W_+\sqrt{t})\right)\end{aligned}$$

with $W_\pm = \frac{\sqrt{D}}{2\delta}|1 \mp \sqrt{1+4\delta^2k^2}|$.